ELSEVIER

International Journal of Solids and Structures 41 (2004) 3735–3746

INTERNATIONAL JOURNAL OF SOLIDS and STRUCTURES

www.elsevier.com/locate/ijsolstr

Three-dimensional vibrations of solid cones with and without an axial circular cylindrical hole

Jae-Hoon Kang [a,*], Arthur W. Leissa [b]

[a] *Department of Architectural Engineering, School of Architecture and Building Science, College of Engineering, Chung-Ang University, 221 Heuksuk-Dong, Dongjak-Ku, Seoul 156 756, South Korea*

[b] *Department of Mechanical Engineering, Colorado State University, Fort Collins, CO, USA*

Received 10 February 2004; received in revised form 10 February 2004

Abstract

A three-dimensional (3-D) method of analysis is presented for determining the free vibration frequencies and mode shapes of solid cones with and without an axial circular cylindrical hole, having arbitrary constraints on their boundaries. The method is based upon the 3-D dynamic equations of elasticity. Displacement components u_r, u_θ, and u_z in the radial, circumferential, and axial directions, respectively, are taken to be sinusoidal in time, periodic in θ, and algebraic polynomials in the r and z directions. Potential (strain) and kinetic energies of the cones are formulated, the Ritz method is used to solve the eigenvalue problem, and upper bound values of the frequencies are obtained by minimizing the frequencies. As the degree of the polynomials is increased, frequencies converge to the exact values. Novel numerical results are presented for solid cones with and without an axial circular cylindrical hole. Convergence to four-digit exactitude is demonstrated for the first five frequencies of the cones.

Keywords: Vibration; Three-dimensional (3-D) analysis; Solid cone; Ritz method

1. Introduction

Three-dimensional (3-D) analysis of structural elements has long been a goal of those who work in the field. With the current availability of computers of increased speed and capacity, it is now possible to perform 3-D structural analyses of bodies to obtain accurate values of static displacements, free vibration frequencies and mode shapes, and buckling loads and mode shapes.

The literature that deals with the free vibration of thick conical shells or cones based upon 3-D analyses is quite limited. The majority of the existing literature describes the vibration analysis for *thin* conical shells, based upon a thin shell or membrane type of shell theory (Leissa, 1973). The first contribution to the 3-D analysis of conical shells was by Leissa and So (1995) applying the Ritz method. Five years later, the conical

* Corresponding author. Tel.: +82-2-820-5342; fax: +82-2-812-4150.
E-mail address: jhkang@cau.ac.kr (J.-H. Kang).

0020-7683/$ - see front matter © 2004 Published by Elsevier Ltd.
doi:10.1016/j.ijsolstr.2004.02.017

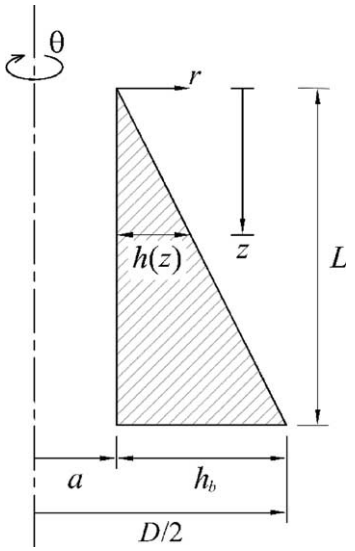

Fig. 1. Right triangular cross-section of a circular cylindrical body of revolution with linearly varying wall thickness and the coordinate system (r, θ, z).

shells were analyzed by a finite element method (Buchanan, 2000; Buchanan and Wong, 2001). However, they all examined the conical shells having *uniform* wall thickness. Some additional study gave some numerical results for linearly varying wall thickness (Leissa and Kang, 1999; Kang and Leissa, 1999). All the above literature is limited to *hollow* truncated cones (i.e., shells). A search of the literature has revealed no 3-D analysis for *solid* cones.

In the present 3-D analysis, the Ritz method is used to obtain accurate frequencies for solid cones with and without an axial circular cylindrical hole. To accommodate these configurations a type of cylindrical coordinate system is used, as shown in Fig. 1, instead of curvilinear coordinates related to the shell mid-surface which were used in the previous publications of the present authors. Although the method itself does not yield exact solutions, proper use of displacement components in the form of algebraic polynomials permits one to obtain frequency upper bounds that are as close to the exact values as desired. Frequencies presented in this work, thus obtained, are very close to their exact values, being exact to four significant figures.

2. Method of analysis

Fig. 1 shows the right triangular cross-section of a circular cylindrical body of revolution with thickness (h) linearly varying in the axial direction (z), and having an inner radius a and an outer radius $D/2$ at the bottom. The cross-section has zero thickness at the top ($z = 0$) and h_b at the bottom ($z = L$), where L is axial length. The curvilinear coordinate system (r, θ, z), also shown in the figure, is used in the analysis. Unlike classical cylindrical coordinates, the radial coordinate (r) is measured from the inner cylindrical surface (instead of the axis), where the inner radius (a) may be as small as desired. The circumferential coordinate (rotation about the axis) is the angle θ. Rotating the cross-section of Fig. 1 one revolution about the axis of revolution ($r = -a$) results in a solid cone with an axial circular cylindrical hole, or a solid cone without a hole when a approaches zero. Thus the valid ranges of the curvilinear coordinates are given for the cone by

$$0 \leqslant r \leqslant h\left(=\frac{h_b}{L}z\right), \quad 0 \leqslant \theta \leqslant 2\pi, \quad 0 \leqslant z \leqslant L. \tag{1}$$

Utilizing tensor analysis (Kang, 1997), the three equations of motion in the curvilinear coordinate system (r, θ, z) were found to be

$$\sigma_{rr,r} + \sigma_{rz,z} + \frac{1}{a+r}(\sigma_{rr} - \sigma_{\theta\theta} + \sigma_{r\theta,\theta}) = \rho\ddot{u}_r, \tag{2a}$$

$$\sigma_{r\theta,r} + \sigma_{\theta z,z} + \frac{1}{a+r}(2\sigma_{r\theta} + \sigma_{\theta\theta,\theta}) = \rho\ddot{u}_\theta, \tag{2b}$$

$$\sigma_{rz,r} + \sigma_{zz,z} + \frac{1}{a+r}(\sigma_{rz} + \sigma_{\theta z,\theta}) = \rho\ddot{u}_z, \tag{2c}$$

where σ_{ij} are the normal ($i = j$) and shear ($i \neq j$) stress components; u_r, u_θ, and u_z are the displacement components in the r, θ, and z directions, respectively; ρ is mass density per unit volume; the commas indicate spatial derivatives; and the dots denote time derivatives.

The well-known relationships between the stress (σ_{ij}) and tensorial strains (ε_{ij}) of isotropic, linear elasticity are

$$\sigma_{ij} = \lambda\varepsilon\delta_{ij} + 2G\varepsilon_{ij}, \tag{3}$$

where λ and G are the Lamé parameters, expressed in terms of Young's modulus (E) and Poisson's ratio (v) for an isotropic solid as:

$$\lambda = \frac{Ev}{(1+v)(1-2v)}, \quad G = \frac{E}{2(1+v)}, \tag{4}$$

$\varepsilon \equiv \varepsilon_{rr} + \varepsilon_{\theta\theta} + \varepsilon_{zz}$ is the trace of the strain tensor, and δ_{ij} is Kronecker's delta.

The three-dimensional (3-D) tensorial strains are found to be related to the three displacements u_r, u_θ, and u_z by (Kang, 1997)

$$\varepsilon_{rr} = u_{r,r}, \quad \varepsilon_{\theta\theta} = \frac{u_{\theta,\theta} + u_r}{a+r}, \quad \varepsilon_{zz} = u_{z,z}, \tag{5a}$$

$$\varepsilon_{r\theta} = \frac{1}{2}\left[u_{\theta,r} + \frac{u_{r,\theta} - u_\theta}{a+r}\right], \quad \varepsilon_{rz} = \frac{1}{2}(u_{r,z} + u_{z,r}), \quad \varepsilon_{\theta z} = \frac{1}{2}\left[u_{\theta,z} + \frac{u_{z,\theta}}{a+r}\right]. \tag{5b}$$

Because the strains are related to the displacement components by Eqs. (5), unacceptable strain singularities may be encountered exactly at $r = 0$ in case of no axial circular cylindrical hole ($a = 0$) due to the term $1/(a+r)$. Such singularities may be avoided by numerically integrating within the volume of the body such that $a \neq 0$ (say, $a/h_b = 10^{-5}$).

During vibratory deformation of the body, its strain (potential) energy (V) is the integral over the domain (Ω):

$$V = \frac{1}{2}\int_\Omega (\sigma_{rr}\varepsilon_{rr} + \sigma_{\theta\theta}\varepsilon_{\theta\theta} + \sigma_{zz}\varepsilon_{zz} + 2\sigma_{r\theta}\varepsilon_{r\theta} + 2\sigma_{rz}\varepsilon_{rz} + 2\sigma_{\theta z}\varepsilon_{\theta z})(a+r)\,\mathrm{d}r\,\mathrm{d}\theta\,\mathrm{d}z. \tag{6}$$

Substituting Eqs. (3) and (5) into Eq. (6) results in the strain energy in terms of the three displacements:

$$V = \frac{1}{2}\int_\Omega \left[\lambda(\varepsilon_{rr} + \varepsilon_{\theta\theta} + \varepsilon_{zz}) + 2G\left\{\varepsilon_{rr}^2 + \varepsilon_{\theta\theta}^2 + \varepsilon_{zz}^2 + 2(\varepsilon_{r\theta}^2 + \varepsilon_{rz}^2 + \varepsilon_{\theta z}^2)\right\}\right](a+r)\,\mathrm{d}r\,\mathrm{d}\theta\,\mathrm{d}z, \tag{7}$$

where the tensorial strains ε_{ij} are defined in terms of the three displacements by Eqs. (5).

The kinetic energy (T) is simply

$$T = \frac{1}{2}\int_{\Omega} \rho(\dot{u}_r^2 + \dot{u}_\theta^2 + \dot{u}_z^2)(a+r)\,\mathrm{d}r\,\mathrm{d}\theta\,\mathrm{d}z. \tag{8}$$

For convenience, the radial r and axial z and coordinates are made dimensionless as:

$$\psi \equiv r/h_\mathrm{b}, \quad \zeta \equiv z/L. \tag{9}$$

Thus the valid ranges of the nondimensional curvilinear coordinates (ψ, θ, ζ) are given by

$$0 \leqslant \psi \leqslant \zeta, \quad 0 \leqslant \theta \leqslant 2\pi, \quad 0 \leqslant \zeta \leqslant 1. \tag{10}$$

For the free, undamped vibration, the time (t) response of the three displacements is sinusoidal and, moreover, the circular symmetry of the body allows the displacements to be expressed by

$$u_r(\psi,\theta,\zeta,t) = U_r(\psi,\zeta)\cos n\theta \sin(\omega t + \alpha), \tag{11a}$$

$$u_\theta(\psi,\theta,\zeta,t) = U_\theta(\psi,\zeta)\sin n\theta \sin(\omega t + \alpha), \tag{11b}$$

$$u_z(\psi,\theta,\zeta,t) = U_z(\psi,\zeta)\cos n\theta \sin(\omega t + \alpha), \tag{11c}$$

where U_r, U_θ, and U_z are displacement functions of ψ and ζ, ω is a natural frequency, and α is an arbitrary phase angle determined by the initial conditions. The circumferential wave number is taken to be an integer ($n = 0, 1, 2, 3, \ldots, \infty$) for a circumferentially closed shell ($0 \leqslant \theta \leqslant 360°$), to ensure periodicity in θ. Then Eqs. (11) account for all free vibration modes except for the torsional ones. These modes arise from an alternative set of solutions which are the same as Eqs. (11), except that $\cos n\theta$ and $\sin n\theta$ are interchanged. For $n > 0$, this set duplicates the solutions of Eqs. (11), with the symmetry axes of the mode shapes being rotated. But for $n = 0$ the alternative set reduces to $u_r = u_z = 0$, $u_\theta = U_\theta^*(r,z)\sin(\omega t + \alpha)$, which corresponds to the torsional modes. The displacements uncouple by circumferential wave number (n), leaving only coupling in r and z.

The Ritz method uses the maximum potential (strain) energy (V_max) and the maximum kinetic energy (T_max) functionals in a cycle of vibratory motion. The functionals are obtained by setting $\sin^2(\omega t + \alpha)$ and $\cos^2(\omega t + \alpha)$ equal to unity in Eqs. (7) and (8) after the displacements (11) are substituted, and by using the nondimensional coordinates ψ and ζ as follows:

$$V_\mathrm{max} = \frac{LG}{2}\int_0^1 \int_0^\zeta \left[\left\{\frac{\lambda}{G}(\kappa_1+\kappa_2+\kappa_3)^2 + 2(\kappa_1^2+\kappa_2^2+\kappa_3^2) + \kappa_4^2\right\}\Gamma_1 + (\kappa_5^2+\kappa_6^2)\Gamma_2\right](a/h_\mathrm{b}+\psi)\,\mathrm{d}\psi\,\mathrm{d}\zeta, \tag{12}$$

$$T_\mathrm{max} = \frac{\omega^2\rho L h_\mathrm{b}^2}{2}\int_0^1 \int_0^\zeta [(U_r^2 + U_z^2)\Gamma_1 + U_\theta^2\Gamma_2](a/h_\mathrm{b}+\psi)\,\mathrm{d}\psi\,\mathrm{d}\zeta, \tag{13}$$

where

$$\kappa_1 \equiv \frac{U_r + nU_\theta}{a/h_\mathrm{b}+\psi}, \quad \kappa_2 \equiv \frac{h_\mathrm{b}}{L}U_{z,\zeta}, \quad \kappa_3 \equiv U_{r,\psi}, \quad \kappa_4 \equiv \frac{h_\mathrm{b}}{L}U_{r,\zeta} + U_{z,\psi}, \tag{14a}$$

$$\kappa_5 \equiv \frac{U_\theta + nU_r}{a/h_\mathrm{b}+\psi} - U_{\theta,\psi}, \quad \kappa_6 \equiv \frac{nU_z}{a/h_\mathrm{b}+\psi} - \frac{h_\mathrm{b}}{L}U_{\theta,\zeta}, \tag{14b}$$

and Γ_1 and Γ_2 are constants, defined by

$$\Gamma_1 \equiv \int_0^{2\pi} \cos^2 n\theta = \begin{cases} 2\pi & \text{if } n = 0, \\ \pi & \text{if } n \geqslant 1, \end{cases} \tag{15a}$$

$$\Gamma_2 \equiv \int_0^{2\pi} \sin^2 n\theta = \begin{cases} 0 & \text{if } n = 0, \\ \pi & \text{if } n \geqslant 1. \end{cases} \tag{15b}$$

It is known that λ and G have the same units as E from Eqs. (4). The nondimensional constant λ/G in Eq. (12) involves only v; i.e.,

$$\frac{\lambda}{G} = \frac{2v}{1-2v}. \tag{16}$$

The displacement functions U_r, U_θ, and U_z in Eqs. (11) are further assumed as

$$U_r(\psi,\zeta) = \eta_r(\psi,\zeta) \sum_{i=0}^{I} \sum_{j=0}^{J} A_{ij} \psi^i \zeta^j \tag{17a}$$

$$U_\theta(\psi,\zeta) = \eta_\theta(\psi,\zeta) \sum_{k=0}^{K} \sum_{l=0}^{L} B_{kl} \psi^k \zeta^l \tag{17b}$$

$$U_z(\psi,\zeta) = \eta_z(\psi,\zeta) \sum_{m=0}^{M} \sum_{n=0}^{N} C_{mn} \psi^m \zeta^n \tag{17c}$$

and similarly for U_θ^*, where i, j, k, l, m, and n are integers; I, J, K, L, M, and N are the highest degrees of the polynomial terms; A_{ij}, B_{kl} and C_{mn} are arbitrary coefficients to be determined, and the η are functions depending upon the geometric boundary conditions to be enforced. For example:

1. Completely free: $\eta_r = \eta_\theta = \eta_z = 1$.
2. Bottom end ($z = L$) fixed, remaining boundaries free: $\eta_r = \eta_\theta = \eta_z = \zeta - 1$.
3. Inner surface ($r = 0$) fixed, remaining boundaries free: $\eta_r = \eta_\theta = \eta_z = \psi$.
4. Outer surface ($r = zh_b/L$) fixed, remaining boundaries free: $\eta_r = \eta_\theta = \eta_z = \psi - \zeta$.
5. Inner surface restrained normally and axially, but not circumferentially:

$$\eta_r = \eta_z = \psi, \quad \eta_\theta = 1.$$

6. Inner surface restrained normally, but not tangentially: $\eta_r = \psi$, $\eta_\theta = \eta_z = 1$.

The functions of η shown above, impose only the necessary geometric constraints. Together with the algebraic polynomials in Eqs. (17), they form function sets which are mathematically complete (Kantorovich and Krylov, 1958, pp. 266–268). Thus, the function sets are capable of representing any 3-D motion of the body with increasing accuracy as the indices $I, J, \ldots, N$ are increased. In the limit, as sufficient terms are taken, all internal kinematic constraints vanish, and the functions (17) will approach the exact solution as closely as desired.

The eigenvalue problem is formulated by minimizing the free vibration frequencies with respect to the arbitrary coefficients A_{ij}, B_{kl} and C_{mn}, thereby minimizing the effects of the internal constraints present, when the function sets are finite. This corresponds to the equations (Ritz, 1909):

$$\frac{\partial}{\partial A_{ij}}(V_{\max} - T_{\max}) = 0 \quad (i = 0, 1, 2, \ldots, I; j = 0, 1, 2, \ldots, J), \tag{18a}$$

$$\frac{\partial}{\partial B_{kl}}(V_{\max} - T_{\max}) = 0 \quad (k = 0, 1, 2, \ldots, K; l = 0, 1, 2, \ldots, L), \tag{18b}$$

$$\frac{\partial}{\partial C_{mn}}(V_{\max} - T_{\max}) = 0 \quad (m = 0, 1, 2, \ldots, M; n = 0, 1, 2, \ldots, N). \tag{18c}$$

Eqs. (18) yield a set of $(I+1)(J+1)+(K+1)(L+1)+(M+1)(N+1)$ linear, homogeneous, algebraic equations in the unknowns A_{ij}, B_{kl}, and C_{mn}. For a nontrivial solution, the determinant of the coefficient matrix is set equal to zero, which yields the frequencies (eigenvalues). These frequencies are upper bounds on the exact values. The mode shape (eigenfunction) corresponding to each frequency is obtained, in the usual manner, by substituting each ω back into the set of algebraic equations, and solving for the ratios of coefficients.

3. Convergence studies

To establish the accuracy of frequencies obtained by the procedure described above, it is necessary to conduct some convergence studies to determine the number of terms required in the power series of Eqs. (17). A convergence study is based upon the fact that all the frequencies obtained by the Ritz method should converge to their exact values in an upper bound manner. If the results do not converge properly, or converge too slowly, it is likely that the assumed displacements may be poor ones, or be missing some functions from a minimal complete set of polynomials.

Table 1 is such a study for the completely free, short ($L/D = 0.2$) solid cone without an axial circular cylindrical hole ($a = 0$), depicted as the outermost configuration in Fig. 2. The table lists the first five nondimensional frequencies in $\omega L\sqrt{\rho/G}$ with $\nu = 0.3$, for mode shapes having two circumferential waves ($n = 2$).

To make the study of convergence less complicated, equal number of polynomial terms were taken in both the r (or ψ) coordinate (i.e., $I = K = M$) and z (or ζ) coordinate (i.e., $J = L = N$), although some computational optimization could be obtained for some configurations and some mode shapes by using unequal number of polynomial terms.

The symbols TR and TZ in the table indicate the total number of polynomial terms used in the r (or ψ) and z (or ζ) directions, respectively. Note that the frequency determinant order DET is related to TR and TZ as follows:

$$\mathrm{DET} = \left\{ \begin{array}{ll} \mathrm{TR} \times \mathrm{TZ} & \text{for torsional modes } (n = 0), \\ 2 \times \mathrm{TR} \times \mathrm{TZ} & \text{for axisymmetric modes } (n = 0), \\ 3 \times \mathrm{TR} \times \mathrm{TZ} & \text{for general modes } (n \geqslant 1). \end{array} \right\} \tag{19}$$

Table 1 shows the monotonic convergence of all five frequencies as TR ($= I+1$, $K+1$, and $M+1$ in Eqs. (17)) is increased, as well as TZ ($= J+1$, $L+1$, and $N+1$ in Eqs. (17)). One sees, for example, that the lowest nondimensional frequency $\omega L\sqrt{\rho/G}$ with $n = 2$ converges to four digits (0.3394) when as few as $3\times(5\times4) = 60$ terms are used, which results in $\mathrm{DET} = 60$. Moreover, this accuracy requires using at least five terms in the radial direction ($\mathrm{TR} = 5$) and four in the axial direction ($\mathrm{TZ} = 4$). Numbers in underlined, bold-face type in Table 1 are the most accurate values (i.e., least upper bounds) achieved with the smallest determinant sizes.

Table 1
Convergence of the five lowest frequencies in $\omega L\sqrt{\rho/G}$ of a completely free, short ($L/D = 0.2$) solid cone ($a = 0$) for $n = 2$ with $\nu = 0.3$

TR	TZ	DET	1	2	3	4	5
2	2	12	0.7467	1.459	3.003	6.488	8.636
2	4	24	0.6777	1.453	2.927	5.772	7.388
2	6	36	0.6738	1.453	2.926	5.749	7.340
2	8	48	0.6734	1.453	2.926	5.748	7.339
3	2	18	0.3526	1.376	2.012	2.061	3.989
3	4	36	0.3443	1.362	1.881	2.017	3.926
3	6	54	0.3443	1.362	1.868	2.017	3.924
3	8	72	0.3443	1.362	1.867	2.017	3.924
4	2	24	0.3481	1.294	1.400	1.989	3.463
4	4	48	0.3395	1.158	1.380	1.984	3.252
4	6	72	0.3394	1.157	1.379	1.984	3.217
4	8	96	0.3394	1.157	1.379	1.984	3.213
5	2	30	0.3481	1.244	1.391	1.974	2.492
5	4	60	**0.3394**	1.107	1.376	1.969	2.193
5	6	90	0.3394	1.107	1.376	1.969	2.187
5	8	120	0.3394	1.107	1.376	1.969	2.187
6	2	36	0.3481	1.241	1.390	1.974	2.316
6	4	72	0.3394	**1.105**	**1.375**	**1.968**	2.052
6	6	108	0.3394	1.105	1.375	1.968	2.051
6	8	144	0.3394	1.105	1.375	1.968	**2.050**

Notes: TR = total numbers of polynomial terms used in the r (or ψ) direction.
TZ = total number of polynomial terms used in the z (or ζ) direction.
DET = frequency determinant order.

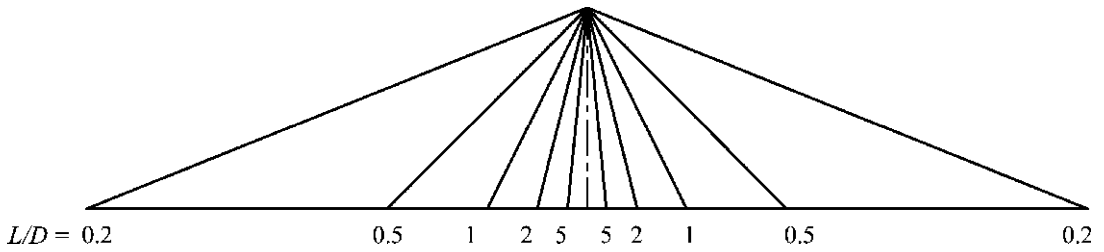

Fig. 2. Solid cones for $L/D = 0.2$, 0.5, 1, 2, and 5.

Table 2 is a similar convergence study for the much more slender ($L/h_b = 10$) solid cone with an axial circular cylindrical hole ($a/h_b = 0.2$) shown at the bottom, right side of Fig. 3. One sees that the lowest frequency (1.670) for $n = 1$ requires using at least (TR,TZ) = (3, 8) for exactitude to four significant figures. Compared with the short solid cone in Table 1, more polynomial terms in the axial direction (TZ) are needed, while less are needed in the radial direction (TR) to obtain the same accuracy in frequencies.

4. Numerical results and discussion

Table 3 presents nondimensional frequencies in $\omega L\sqrt{\rho/G}$ of completely free, solid cones *without* an axial circular cylindrical hole ($a = 0$) for $L/D = 0.2$, 0.5, 1, 2, and 5. These configurations are depicted in Fig. 2.

Table 2
Convergence of the five lowest frequencies in $\omega L\sqrt{\rho/G}$ of a completely free, slender ($L/h_b = 10$) cone *with* an axial circular cylindrical hole ($a/h_b = 0.2$) for $n = 1$ with $\nu = 0.3$

TR	TZ	DET	1	2	3	4	5
2	2	12	17.21	26.49	27.95	42.13	47.29
2	4	24	1.713	5.863	18.83	23.60	26.12
2	6	36	1.684	3.763	6.517	13.76	20.69
2	8	48	1.682	3.627	6.036	9.498	13.30
2	10	60	1.682	3.627	5.992	8.623	11.50
2	11	66	1.682	3.627	5.990	8.606	11.40
2	12	72	1.682	3.627	5.990	8.597	11.35
2	13	78	1.682	3.627	5.990	8.596	11.32
3	2	18	16.97	26.15	27.81	39.23	45.17
3	4	36	1.698	5.658	18.48	23.21	26.00
3	6	54	1.672	3.732	6.445	13.36	20.29
3	8	72	**1.670**	3.602	5.986	9.374	13.19
3	10	90	1.670	3.601	5.949	8.558	11.39
3	11	99	1.670	3.601	5.947	8.540	11.31
3	12	108	1.670	3.601	5.946	8.532	11.25
3	13	117	1.670	3.601	5.946	8.531	11.23
4	2	24	16.88	25.51	27.56	39.01	42.17
4	4	48	1.695	5.560	18.31	22.87	25.61
4	6	72	1.672	3.726	6.422	13.09	20.07
4	8	96	1.670	3.600	5.978	9.316	13.14
4	10	120	1.670	3.600	5.944	8.547	11.36
4	11	132	1.670	**3.599**	5.942	8.529	11.29
4	12	144	1.670	3.599	**5.941**	8.521	11.23
4	13	156	1.670	3.599	5.941	8.521	**11.21**
5	2	30	16.85	25.50	27.55	38.84	41.95
5	4	60	1.695	5.531	18.26	22.78	25.58
5	6	90	1.672	3.724	6.414	12.97	19.97
5	8	120	1.670	3.600	5.976	9.295	13.12
5	10	150	1.670	3.599	5.943	8.545	11.35
5	11	165	1.670	3.599	5.941	8.527	11.29
5	12	180	1.670	3.599	5.941	**8.520**	11.23
5	13	195	1.670	3.599	5.941	8.520	11.21

Notes: TR = total number of polynomial terms used in the r (or ψ) direction.
TZ = total number of polynomial terms used in the z (or ζ) direction.
DET = frequency determinant order.

Poisson's ratio (ν) was taken to be 0.3. Thirty-five frequencies are given for each configuration, which are arise from seven circumferential wave numbers ($n = 0^T, 0^A$, 1, 2, 3, 4, 5) and the first five frequencies ($s = 1$, 2, 3, 4, 5) for each value of n, where the superscripts T and A indicate torsional and axisymmetric modes, respectively. The numbers in parentheses identify the first five frequencies for each configuration. The zero frequencies of rigid body modes are omitted from the table.

Table 4 presents nondimensional frequencies in $\omega L\sqrt{\rho/G}$ of completely free cones *with* an axial circular cylindrical hole ($a/h_b = 0.2$) for $L/h_b = 0.4$, 1, 2, 4, and 10. These configurations are shown in Fig. 3. Poisson's ratio (ν) was also taken to be 0.3. All the configurations shown in Fig. 3 are exactly the same as those in Fig. 2 if the radius (a) of the circular holes approaches zero. Thus $L/h_b = 0.4$, 1, 2, 4, and 10 in Fig. 3 correspond to $L/D = 0.2$, 0.5, 1, 2, and 5 in Fig. 2, respectively, if the sides were moved inwards to close the holes.

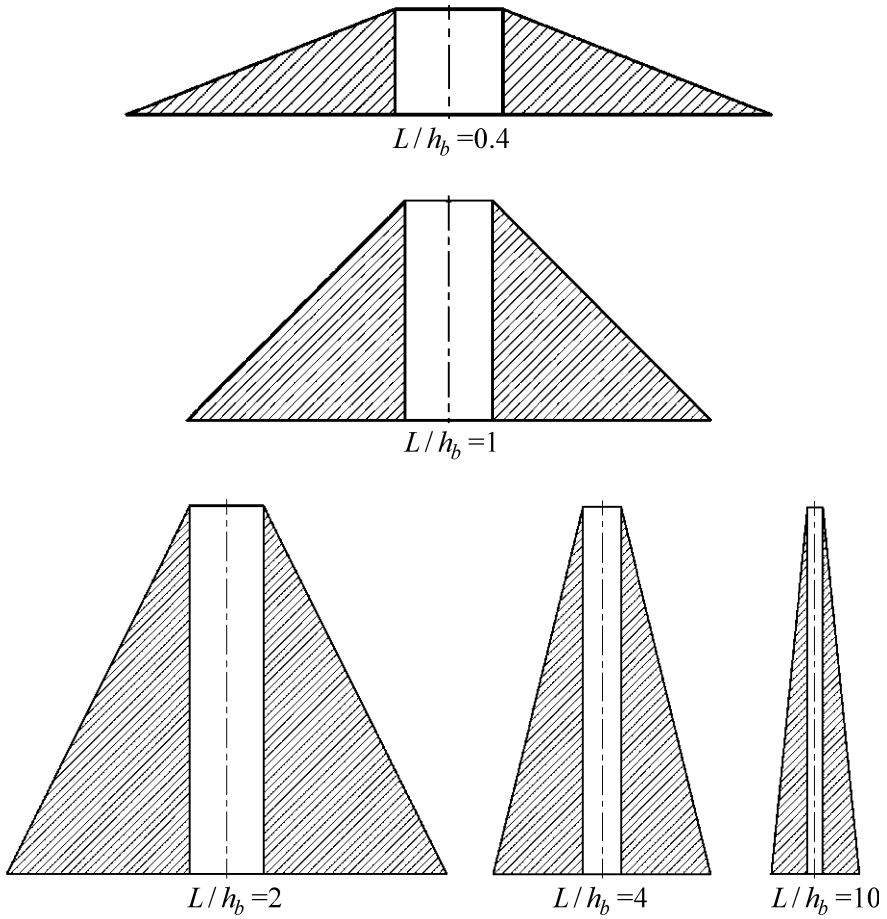

Fig. 3. Cones with axial circular cylindrical holes ($a/h_b = 0.2$) for $L/h_b = 0.4$, 1, 2, 4, and 10.

It is seen from Tables 3 and 4 that for *short* ($L/D \leqslant 1$ or $L/h_b \leqslant 2$) cones the fundamental (lowest) frequency is for modes having two ($n = 2$) circumferential half-waves, while for *long and slender* ($L/D \geqslant 2$ or $L/h_b \geqslant 4$) ones the fundamental one is for $n = 1$. That is, for these more slender configurations the lowest frequencies correspond to bending modes of beams of length L. Tables 3 and 4 also show that as the cones become more long and slender ($L/D \geqslant 1$ or $L/h_b \geqslant 2$) the torsional modes ($n = 0^T$) are seen to be significant, each having one such mode among the first five. It is noticed that all the frequencies for the solid cones without a hole are larger than the ones for the cones with a hole, as expected, except for the modes of $n = 1$ of long and slender cones ($L/D = 2$ and 5 or $L/h_b = 4$ and 10). This is because the ones with holes have greater total mass, and also because the hole tends to decrease the stiffness of the body for the modes of the short cones, but increases it greatly for the beam bending modes ($n = 1$) of the slender cones.

5. Concluding remarks

A three-dimensional (3-D) method of analysis has been presented for determining the free vibration frequencies and mode shapes of solid cones with and without an axial circular cylindrical hole having

Table 3
Frequencies in $\omega L\sqrt{\rho/G}$ of completely free, solid cones ($a = 0$) for $\nu = 0.3$

n	s	L/D				
		0.2	0.5	1	2	5
0^{T}	1	2.066	4.314	**5.334(3)**	**5.647(3)**	**5.744(4)**
	2	3.390	6.338	8.371	8.911	9.065
	3	4.623	8.072	11.12	12.07	12.28
	4	5.125	8.772	12.57	15.19	15.47
	5	5.997	10.81	14.42	18.30	18.64
0^{A}	1	**0.5381(3)**	**2.335(3)**	**5.384(4)**	**6.971(4)**	7.203
	2	1.268	4.306	6.606	11.35	12.34
	3	1.901	4.939	8.618	12.13	17.33
	4	2.172	6.180	10.44	15.04	22.15
	5	3.170	7.783	11.87	17.74	26.67
1	1	**0.8077(5)**	**3.002(4)**	**3.988(2)**	**2.886(1)**	**1.353(1)**
	2	1.265	3.315	5.769	**5.241(2)**	**2.654(2)**
	3	1.650	4.554	6.886	**7.663(5)**	**4.224(3)**
	4	2.594	5.452	7.274	9.810	**6.029(5)**
	5	2.627	6.483	8.918	11.64	8.032
2	1	**0.3394(1)**	**1.566(1)**	**3.881(1)**	8.357	21.36
	2	1.105	3.295	6.215	11.47	26.14
	3	1.375	4.467	9.254	15.60	30.75
	4	1.967	4.831	9.564	16.81	33.79
	5	2.041	6.781	10.57	18.42	37.58
3	1	**0.5048(2)**	**2.319(2)**	**5.763(5)**	12.50	32.29
	2	1.385	4.772	9.037	16.91	39.38
	3	1.994	5.503	11.89	21.36	44.59
	4	2.403	6.508	12.46	21.96	47.95
	5	2.651	8.123	13.64	24.61	51.12
4	1	**0.6591(4)**	**3.017(5)**	7.498	16.32	42.65
	2	1.653	6.011	11.48	21.65	51.23
	3	2.509	6.515	14.13	26.22	57.18
	4	2.769	8.170	15.45	26.88	60.42
	5	3.332	9.379	16.53	30.29	64.40
5	1	0.8095	3.695	9.194	20.02	53.15
	2	1.918	7.156	13.74	26.07	63.29
	3	2.981	7.522	16.35	30.65	69.88
	4	3.155	9.768	18.14	31.71	72.94
	5	3.996	10.62	19.42	35.37	77.24

Notes: T = torsional mode; A = axisymmetric mode.
Numbers in parentheses identify frequency sequence.

arbitrary constraints on their boundaries. The 3-D equations of the theory of elasticity are used in their general forms for isotropic, homogeneous materials, with the corresponding energy functionals. They are only limited to small strains. No other constraints are placed upon the displacements.

Numerical results for frequencies were presented for several completely free cones. The frequencies are exact up to four significant figures for the lower frequencies for the size of determinants used (approximately 150); but if greater accuracy is needed, especially for the higher frequencies, larger determinants would be required. Nevertheless, these determinant sizes are at least one order of magnitude less than those that would be required for equivalent accuracy by finite element analysis.

Table 4
Frequencies in $\omega L\sqrt{\rho/G}$ of completely free cones *with* axial circular cylindrical holes ($a/h_b = 0.2$) for $\nu = 0.3$

n	s	L/h_b				
		0.4	1	2	4	10
0^T	1	1.746	3.655	**4.520(5)**	**4.782(2)**	**4.862(3)**
	2	2.923	5.426	7.240	7.705	7.834
	3	4.048	6.947	9.692	10.65	10.83
	4	4.433	7.638	10.80	13.62	13.86
	5	5.316	9.599	12.82	16.62	16.92
0^A	1	**0.4280(3)**	**1.881(2)**	**4.381(4)**	**6.325(4)**	**6.563(5)**
	2	1.034	3.257	5.580	9.347	11.51
	3	1.375	4.145	7.087	10.44	16.30
	4	1.838	5.451	8.531	12.72	20.79
	5	2.754	6.067	9.898	14.62	23.67
1	1	**0.6576(5)**	2.574	**3.907(2)**	**3.212(1)**	**1.670(1)**
	2	1.084	2.661	4.945	**5.785(3)**	**3.599(2)**
	3	1.280	3.739	5.459	7.903	**5.941(4)**
	4	1.975	4.722	6.568	9.505	8.520
	5	2.396	5.394	8.255	10.26	11.21
2	1	**0.2473(1)**	**1.163(1)**	**2.939(1)**	**6.340(5)**	12.09
	2	0.8420	**2.159(4)**	**4.267(3)**	7.990	16.29
	3	0.9204	3.529	5.478	8.110	18.91
	4	1.547	3.762	6.874	10.09	21.50
	5	1.654	4.432	7.753	11.13	21.57
3	1	**0.4168(2)**	**1.920(3)**	4.777	10.37	26.75
	2	1.144	3.883	7.392	13.87	27.50
	3	1.613	4.565	9.841	15.25	32.44
	4	1.982	5.339	10.11	17.30	36.52
	5	2.175	6.289	10.61	18.13	39.11
4	1	**0.5490(4)**	**2.513(5)**	6.247	13.59	35.24
	2	1.377	4.999	9.535	18.00	42.39
	3	2.086	5.424	11.71	21.77	47.08
	4	2.293	6.791	12.79	22.33	49.24
	5	2.771	7.719	13.67	24.37	49.78
5	1	0.6745	3.079	7.651	16.66	43.52
	2	1.597	5.956	11.43	21.70	51.61
	3	2.483	6.258	13.53	25.50	56.74
	4	2.593	8.130	15.03	26.35	59.49
	5	3.328	8.740	16.04	29.28	62.70

Notes: T = torsional mode; A = axisymmetric mode.
Numbers in parentheses identify frequency sequence.

Results were presented for completely free cones. However, as described in Section 2, the procedure could also be used for cones having constraints at one or more of the cone surfaces.

References

Buchanan, G.R., 2000. Vibration of truncated conical cylinders of crystal class 6/mmm. Journal of Vibration and Control 6, 985–998.
Buchanan, G.R., Wong, F.T.-I., 2001. Frequencies and mode shapes for thick truncated hollow cones. International Journal of Mechanical Sciences 43, 2815–2832.

Kang, J.-H., 1997. Three-dimensional vibration analysis of thick shells of revolution with arbitrary curvature and variable thickness. Ph.D. Dissertation. Ohio State University, Columbus, Ohio.

Kang, J.-H., Leissa, A.W., 1999. Three-dimensional vibrations of hollow cones and cylinders with linear thickness variations. Journal of the Acoustical Society of America 106 (2), 748–755.

Kantorovich, L.V., Krylov, V.I., 1958. Approximate Methods in Higher Analysis. Noordhoff, Gronigen, The Netherlands.

Leissa, A.W., 1973. Vibration of Shells. NASA SP 388, The US Government Printing Office, Washington, DC. Reprinted 1993, by The Acoustical Society of America.

Leissa, A.W., Kang, J.-H., 1999. Three-dimensional vibration analysis of thick shells of revolution. Journal of Engineering Mechanics 125 (12), 1365–1371.

Leissa, A.W., So, J., 1995. Three-dimensional vibrations of truncated hollow cones. Journal of Vibration and Control 1, 145–158.

Ritz, W., 1909. Über eine neue Methode zur Lösung gewisser. Variationsprobleme der mathematischen Physik 135, 1–61.